

Plant Sunscreens in the UV-B: Ultraviolet Spectroscopy of Jet-Cooled Sinapoyl Malate, Sinapic Acid, and Sinapate Ester Derivatives

Jacob C. Dean,[†] Ryoji Kusaka,[†] Patrick S. Walsh,[†] Florent Allais,^{‡,§,||} and Timothy S. Zwier^{*,†}

[†]Department of Chemistry, Purdue University, West Lafayette, Indiana 47907-2084, United States

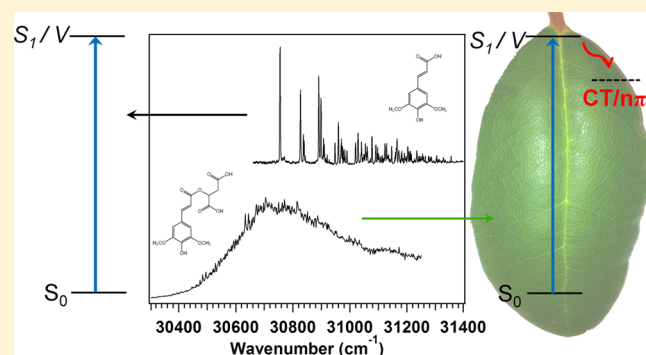
[‡]AgroParisTech, Chaire Agro-Biotechnologies Industrielles (ABI), 247 rue Paul Vaillant-Couturier, F-51100 Reims, France

[§]AgroParisTech, UMR 782 GMPA, Site de Grignon, F-78850 Thiverval-Grignon, France

^{||}INRA, UMR 782 GMPA, Site de Grignon, F-78850 Thiverval-Grignon, France

S Supporting Information

ABSTRACT: Ultraviolet spectroscopy of sinapoyl malate, an essential UV-B screening agent in plants, was carried out in the cold, isolated environment of a supersonic expansion to explore its intrinsic UV spectral properties in detail. Despite these conditions, sinapoyl malate displays anomalous spectral broadening extending well over 1000 cm^{-1} in the UV-B region, presenting the tantalizing prospect that nature's selection of UV-B sunscreen is based in part on the inherent quantum mechanical features of its excited states. Jet-cooling provides an ideal setting in which to explore this topic, where complications from intermolecular interactions are eliminated. In order to better understand the structural causes of this behavior, the UV spectroscopy of a series of sinapate esters was undertaken and compared with *ab initio* calculations, starting with the simplest sinapate chromophore sinapic acid, and building up the ester side chain to sinapoyl malate. This “deconstruction” approach provided insight into the active mechanism intrinsic to sinapoyl malate, which is tentatively attributed to mixing of the bright V (${}^1\pi\pi^*$) state with an adiabatically lower ${}^1n\pi^*$ state which, according to calculations, shows unique charge-transfer characteristics brought on by the electron-rich malate side chain. All members of the series absorb strongly in the UV-B region, but significant differences emerge in the appearance of the spectrum among the series, with derivatives most closely associated with sinapoyl malate showing characteristic broadening even under jet-cooled conditions. The long vibronic progressions, conformational distribution, and large oscillator strength of the V ($\pi\pi^*$) transition in sinapates makes them ideal candidates for their role as UV-B screening agents in plants.



1. INTRODUCTION

UV-B radiation comprises the 280–315 nm region of the solar spectrum, and despite its comparatively small contribution to the spectrum, its deleterious effects on higher plant life and function are substantial. Defensive measures to protect susceptible plant cells/tissues are therefore necessary, given that plants sustain constant exposure to such radiation. As such, the impact of UV-B light on plant growth and sustainability has been the subject of recent research.^{1–5} Among the negative consequences of UV-B exposure is oxidative damage following free radical formation that leads to the destruction of DNA and tissues, which ultimately affects the integrity of the plant structure and inhibits plant growth.^{1–3,6} Additionally, disruptions in the efficiency of photosynthesis, flowering, and transpiration have been documented.^{7,8} As a means of alleviating these harmful effects, many plants utilize screening agents, such as phenolics, generated by natural biosynthetic pathways and fine-tuned to absorb those destructive photons. These molecules are transported into the upper epidermal layer of leaves or seedlings, where they accumulate in relatively high

concentration to prevent penetration of UV-B radiation into the underlying mesophyll layer where photosynthesis occurs.^{1,9} Using genetic mutations in the *Arabidopsis thaliana* plant, it was found that the phenylpropanoid pathway could be manipulated to reduce levels of sinapate esters, resulting in a corresponding increase in UV-B sensitivity.^{1–3,9–12} Such experiments provide unequivocal evidence to implicate sinapate esters (or sinapates) as the primary class of molecules screening UV-B in *Brassicaceae* plants, using such observables as plant growth/injury,³ fluorescence analysis of sinapates and chlorophyll,^{10,12} and photosynthetic activity.² Sinapate esters are ester derivatives of sinapic acid, and sinapoyl malate is the dominant species concentrated in the leaf epidermis of adult *Arabidopsis* plants.^{9,10,13} The chemical structures of these molecules are shown in Figure 1a.

In order for sinapoyl malate/sinapate esters to act as effective UV-B protectants, they not only must be present in sufficient

Received: June 17, 2014

Published: October 8, 2014

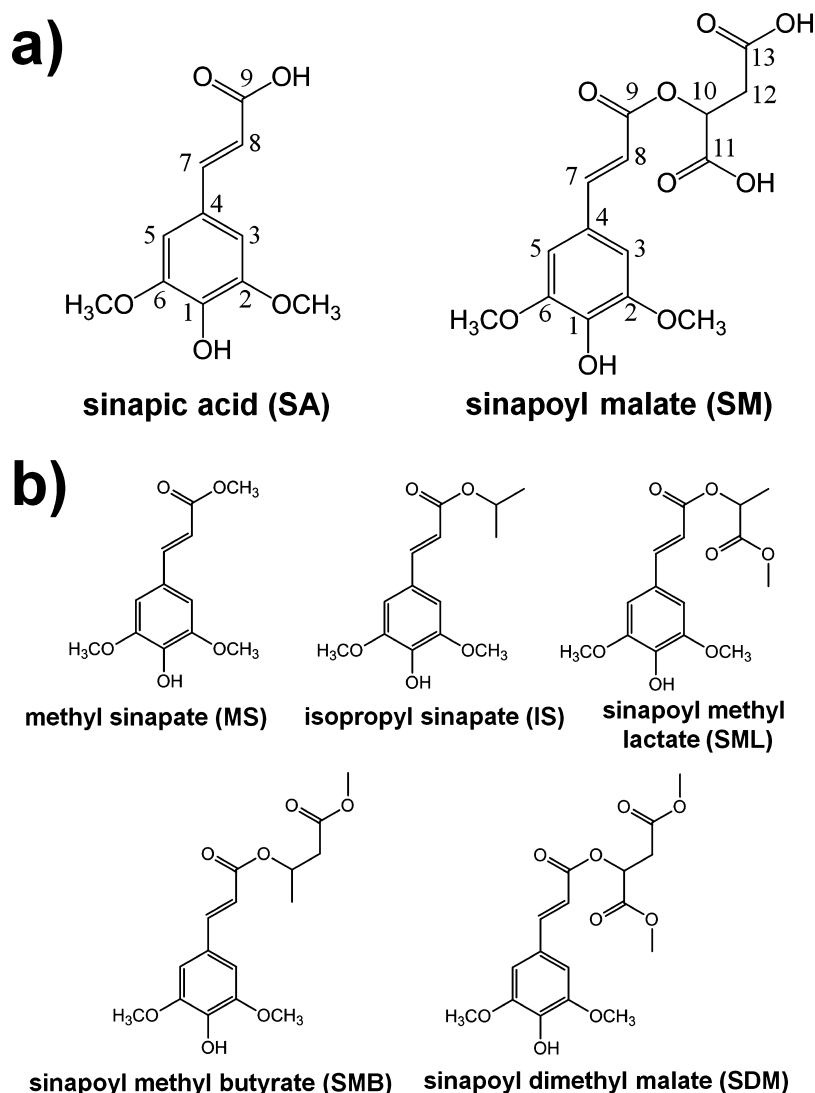


Figure 1. Chemical structures for the full series of molecules studied including (a) sinapic acid (SA) and sinapoyl malate (SM) and (b) sinapate derivatives that bridge between these two in chemical complexity, including methyl sinapate (MS), isopropyl sinapate (IS), sinapoyl methyl-lactate (SML), sinapoyl methyl-butyrates (SMB), and sinapoyl dimethyl malate (SDM). All samples were studied in stereochemically pure (*S*) form.

abundance and uniformly distributed in the upper epidermis of plant leaves but must also be able to absorb across much of the UV-B and with high extinction coefficients.^{10,12} While the natural occurrence of biosynthetic pathways that produce these molecules and their basic UV absorption properties mark them as candidate UV-B sunscreens, a detailed investigation of the intrinsic UV absorption properties and excited states of these compounds has yet to be undertaken. By introducing these molecules into the cold, isolated environment of a supersonic expansion, their fundamental absorption properties can be explored in detail free from solvent effects or other environmental perturbations. By employing this technique, the intrinsic UV spectroscopy of sinapoyl malate and various smaller sinapate derivatives are assessed in detail here.

Another class of molecules that is chemically related to sinapates, and therefore represents a relevant set of analogues, are the cinnamates. These differ from sinapates only by the lack of methoxy substituents on the aromatic ring *meta* to the vinyl group, and at times a change in substitution of the *para* hydroxy group depending on the derivatization. The UV spectroscopy of cinnamate derivatives and their photophysical characteristics

have been characterized extensively in solution,^{14–19} and the derivative octyl methoxycinnamate is a chief ingredient in synthetic/cosmetic UV-B sunscreens. Excited state decay mechanisms from the excited ${}^1\pi\pi^*$ state in the cinnamate class of molecules include internal conversion to the ground state, *trans*–*cis* photoisomerization followed by internal conversion, and internal conversion to a lower ${}^1n\pi^*$ state.^{14–17} Gas phase jet studies of the sunscreen octyl methoxycinnamate (or 2-ethylhexyl-4-methoxycinnamate, EHMC) and the simpler derivative methyl-4-methoxycinnamate (MMC) were recently undertaken by Buma and co-workers, and their results revealed picosecond ${}^1\pi\pi^*$ state lifetimes (based on resonant two-photon ionization line widths) yet nanosecond decay profiles for the two-photon ionization yield.²⁰ These results were interpreted as signaling fast internal conversion to an adiabatically lower ${}^1n\pi^*$ state (picoseconds), which then decayed on a nanosecond time scale. Such fast internal conversion to an adiabatically lower ${}^1n\pi^*$ state was previously characterized in the similar hydroxy-substituted cinnamates, *p*-coumaric acid (pCA) and its methyl ester (4-hydroxycinnamate, MeOpCA), by similar experimental

methods, and further confirmed by quantum chemical calculations.^{21–23} Finally, picosecond pump–probe measurements and symmetry-adapted cluster-configuration interaction (SAC-CI) calculations of MeOpCA performed by Shimada et al. indicate the possibility of excited state *trans*–*cis* isomerization about the propenyl double bond as an additional/alternative pathway giving rise to the broadening observed in the UV spectrum of MeOpCA.²⁴

In this work, the UV spectroscopy of a series of sinapate esters is thoroughly investigated. The nature of the strong ${}^1\pi\pi^*$ electronic transition responsible for UV-B screening is analyzed via the vibrationally resolved UV spectra that are afforded by cooling the molecules in a supersonic expansion. The series presented here includes the simplest sinapate chromophore, sinapic acid (SA), and the biologically relevant sinapoyl malate (SM) (neutral diacid). In addition, the UV spectroscopy of a sequence of increasingly complex ester derivatives was carried out to test the sensitivity of the spectroscopy to various aspects of the structure of sinapoyl malate. These include methyl sinapate (MS), isopropyl sinapate (IS), sinapoyl methyl-lactate (SML), sinapoyl methyl-butyrate (SMB), and the dimethyl ester of sinapoyl malate (sinapoyl dimethyl malate, SDM) which are shown in Figure 1b. When possible, single-conformation UV spectra were attained for those conformers populated in the expansion, and in all cases, two major conformers were observed in nearly equal abundance. Conformation-specific IR spectroscopy was performed on SA, SM, and SDM in the OH stretch (3500–3700 cm^{-1}), alkyl CH stretch (2800–3050 cm^{-1}), and “mid-IR” (1100–1900 cm^{-1}) regions, to confirm the structures of those conformational isomers. Of the series of molecules presented, sinapoyl malate (and its dimethyl derivative) yielded a distinctly broadened spectrum, suggesting the possibility of excited state processes at play. Several mechanisms which could give rise to such anomalous broadening in the gas phase are discussed, leading to a tentative assignment for the broadening to excited state mixing of the bright $\pi\pi^*$ state with a nearby $n\pi^*$ state with substantial charge-transfer character, which is uniquely present and active in the UV-B region in sinapoyl malate.

2. EXPERIMENTAL SECTION

2.1. Experimental Methods. Sinapic acid was purchased from Sigma-Aldrich, while all other samples were synthesized. Synthesis of sinapoyl malate (2-*O*-sinapoyl-L-malate) was performed from the procedure reported in Quentin et al. and Allais et al.^{25,26} Detailed synthetic procedures for MS, IS, SML, SMB, and SDM are given in the Supporting Information. All of the chiral samples (SML, SMB, SM, and SDM) were synthesized in stereochemically pure form with *S*-chirality, as is the case for naturally abundant sinapoyl malate. SA, SMB, SM, and SDM were all introduced into the gas phase by laser desorption from a thin film of the solid on a graphite surface, necessitated due to extensive decomposition upon heating those samples. A detailed description of the laser desorption source can be found elsewhere,²⁷ but a brief description is given in the Supporting Information. MS, IS, and SML were heated in a sample oven behind a Parker Series 9 general valve, to temperatures of 60, 160, and 190 °C, respectively, to generate sufficient vapor pressure for the experiment. In this case, neon or helium was used as the buffer gas at a backing pressure of 2–3 bar, instead of argon as used for laser desorption. The vaporized sample was entrained in the buffer gas, forming a supersonic expansion, which was then skimmed upon entry into the extraction region of a time-of-flight mass spectrometer to form a molecular beam.

UV excitation spectra were obtained via resonant two-photon ionization (R2PI) in either a one-color (SA, MS, IS, SM, SDM; 1C-R2PI) or two-color (SML, SMB, SDM; 2C-R2PI) scheme. For 2C-

R2PI measurements, two laser pulses were spatially and temporally overlapped, and the frequency of the excitation photon was scanned while the ionization photon remained fixed at a frequency lower than the UV absorption. For 1C-R2PI, UV pulse energies of $\sim 100 \mu\text{J}$ /pulse were used, while 2C-R2PI was performed with $\lambda_{\text{excitation}} \sim 10 \mu\text{J}$ /pulse and $\lambda_{\text{ionization}} \sim 100 \mu\text{J}$ /pulse. Pulse energies were optimized to ensure that saturation effects were minimized. UV–UV holeburning (UV–UV HB) spectroscopy was carried out to obtain conformation-specific spectra of the conformers present in the expansion. Conformation-specific IR spectroscopy was executed by resonant ion-dip infrared spectroscopy (RIDIRS) on SA, SM, and SDM in the OH stretch, alkyl CH stretch, and mid-IR regions. Experimental details of the implementation of these techniques can be found in the Supporting Information. Dispersed fluorescence (DFL) spectra were recorded for the electronic origin transitions of MS and SML by collecting the fluorescence emission, focusing it into the entrance slit (slit width of 50 or 100 μm) of a Horiba Jobin Yvon 750 monochromator, which disperses it onto an intensified charge coupled device (iCCD, Andor iStar).

2.2. Computational Methods. To classify the possible conformational minima for each molecule, a conformational search was carried out using the Amber* or molecular mechanics force field (MMFF) in the MacroModel suite of programs.^{28,29} The first 50–100 conformational minima (or all possible minima if less than 100) were further optimized by density functional theory (DFT) using the M05-2X hybrid functional³⁰ with the 6-31+G(d) basis set. Ground state vibrational frequencies and vertical excitation energies were calculated for all optimized structures using time-dependent DFT (TDDFT) at the same level of theory. S_1 geometries and vibrational frequencies were also calculated for the assigned conformations. All DFT calculations were performed in the Gaussian 09 suite.³¹ For comparison with experimental IR spectra, the calculated harmonic vibrational frequencies were scaled by 0.949, 0.931, and 0.960 for OH stretch, alkyl CH stretch, and mid-IR vibrations as determined previously for this level of theory.^{27,32} The alkyl CH stretch frequencies were scaled to match the equatorial methoxy CH stretch transition in guaiacol near 3015 cm^{-1} .

3. RESULTS AND ANALYSIS

The lowest singlet excitation calculated for the sinapate chromophore is a $\pi\pi^*$ transition characterized predominantly as a HOMO \rightarrow LUMO transition. The energy of this transition falls near the red edge of the UV-B. An overview of the R2PI spectra in this region for the seven molecules in this series is shown in Figure 2. The spectra extend some 1200 cm^{-1} in total, with the origin transitions spanning a range of 350 cm^{-1} depending on the side chain substitution. All of the spectra display considerable Franck–Condon activity, giving rise to fairly congested UV spectra. As the ester side chain becomes increasingly complex (going down the series in Figure 2), the profile of the UV spectrum begins to change with increasing levels of congestion, accompanied by a shift of the intensity distribution toward the blue (from the respective origin transitions). Interestingly, all of the simpler derivatives display sharp, resolved spectra, whereas sinapoyl malate and its methyl ester derivative (SM, SDM) both exhibit broad, featureless spectra that extend well over 1000 cm^{-1} . This observation is of direct interest to nature’s choice of sinapoyl malate as a UV sunscreen for plants, and could signal the presence of excited state dynamics in sinapoyl malate that is different from those of the simpler molecules. The derivatives in the middle of the figure (SML and SMB), substituted with separate halves of the malate side chain, represent an intermediate between the sharp, well-resolved spectra (sinapic acid, methyl sinapate, and isopropyl sinapate) and the broad sinapoyl malate spectra. In these spectra, sharp transitions are clearly observable, but a shift

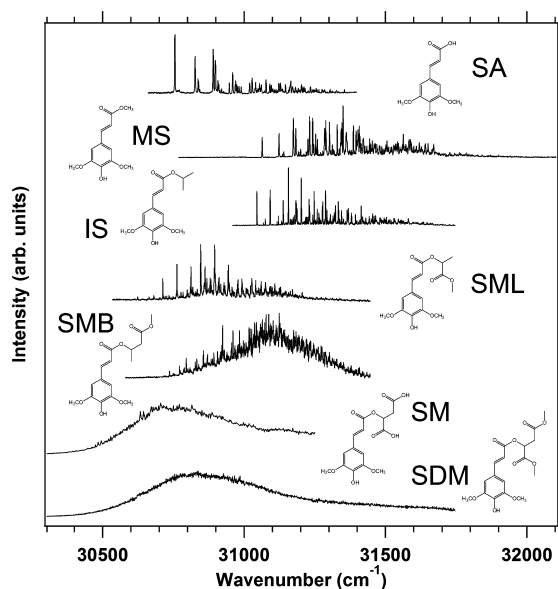


Figure 2. Summary of the R2PI spectra of the sinapate series. The spectra are plotted with increasing side chain derivatization from top to bottom.

in the intensities and the partially resolved nature of the SMB spectrum indicate properties intermediate to those of sinapoyl malate. Detailed analyses of these spectra are given in the following sections.

3.1. Sinapic Acid (SA) Spectroscopy. The simplest of the sinapate series and the biological precursor to sinapoyl malate is sinapic acid. We consider in some detail the UV spectroscopy and conformational assignments of SA as a foundation for the comparisons with other sinapate esters in what follows.

3.1.1. Conformation-Specific UV Spectroscopy. The R2PI spectrum and UV–UV HB spectra for sinapic acid are shown in Figure 3a. Only two conformers were present in the expansion, as proven by UV–UV HB, with very similar appearance and Franck–Condon activity. Their electronic origins (30756 cm^{-1} for A and 30891 cm^{-1} for B) are separated by 135 cm^{-1} . The calculated low-energy minima are planar in the ground state, classifying it in the C_s symmetry group. As can be seen from the transitions labeled in the spectra in Figure 3a, essentially all the Franck–Condon activity can be ascribed to progressions and combination bands involving four vibrational modes: the in-plane C_4 – C_7 = C_8 bending mode, “b”, the C_7 = C_8 – C_9 (O) in-plane scissor mode (S) at 193 cm^{-1} , and even overtones and combinations of the out-of-plane butterfly (β) and C_4 C_7 torsion/symmetric methoxy torsion (τ). The form of these modes is shown in Figure 3b. The presence of only even overtones in the out-of-plane modes proves that the $\pi\pi^*$ excited state is also planar. The close proximity of the β_0^2 and τ_0^2 overtones with the b_0 fundamental suggests the possibility that these levels may be in Fermi resonance with one another. In addition, calculations predict large changes in frequency and form of the low-frequency out-of-plane vibrations of sinapic acid, which could lead to Duschinsky mixing.^{33,34} The experimental and calculated vibrational frequencies for conformers A and B are given in the Supporting Information (Table S1).

The long Franck–Condon progression in the C_4 – C_7 = C_8 bending mode can be rationalized on the basis of the change in the electronic configuration between the ground and excited

states. The HOMO and LUMO molecular orbitals (MOs) are shown in Figure 4a, and they reveal a change in bonding character across the C_4 – C_7 and C_7 – C_8 bonds, with increased double bond character in the former at the expense of double-bond character in the latter. This leads to a quinoidal geometry change evidenced by the large increase in the C_7 – C_8 bond length from 1.34 to 1.40 \AA and a corresponding decrease in the C_4 – C_7 bond length, as shown in Figure 4b. An analogous geometry change was found in the simpler analogue styrene.³⁵

Only three conformational degrees of freedom (Figure 4c) are needed to describe the conformational preferences of sinapic acid. The relative orientations of C_7 = C_8 and C_9 =O groups have the most impact on the energies of the minima, with the *cis* ($C_7C_8C_9=O \sim 0^\circ$) family falling lower in energy by approximately 3 kJ/mol than the *trans* family. Within these families, *syn/anti* combinations arise from separate minima associated with the syringyl OH/ C_7 = C_8 orientation. Interestingly, the calculations predict minima for completely planar, C_s structures, and structures in which the non-H-bonded methoxy CH_3 group is out-of-plane by $\sim 70^\circ$ (at a cost of $\sim 2.3\text{ kJ/mol}$). However, there is no experimental evidence for population in the nonplanar methoxy structures in any of the sinapate esters, suggesting that collisional cooling to the planar minima is complete. The lowest energy conformers are therefore the planar *syn/cis* (0.28 kJ/mol) and *anti/cis* (0.00 kJ/mol) structures differing only by a 180° internal rotation of the OH group. In what follows, we assign conformers A and B as *syn/cis* and *anti/cis*, respectively. These structures are shown in Figure 4c.

3.1.2. RIDIR Spectroscopy. To evaluate the structures of conformers A and B in sinapic acid, single-conformation IR spectra were recorded in the OH stretch, CH stretch, and mid-IR regions using RIDIR spectroscopy (Figure 5). Two OH stretch fundamentals are expected due to the H-bonded phenol (or syringyl) OH and free carboxylic acid, which are predicted to be within 10 cm^{-1} of one another. The presence of a single band in the experimental spectrum (Figure 5, right) suggests that these frequencies are accidentally degenerate.

The CH stretch spectra are very similar to the syringol spectrum in this region,³⁶ showing three sets of bands associated with the three OCH_3 CH vibrations (CH^{eq} , CH_2^{ax} antisymmetric stretch [AS], and CH_3^{ax} symmetric stretch [SS]), which are shifted and split due to Fermi resonances with the CH bend overtones. Slight differences are observed in the AS and SS OCH_3 bands between the two conformers. In conformer A, four bands are clearly observed in the AS OCH_3 region, whereas in B the splittings are less resolved. Of greatest relevance for the sinapate esters studied here, the lowest-frequency SS OCH_3 bands at $\sim 2850\text{ cm}^{-1}$ show different intensities for the H-bonded and non-H-bonded OCH_3 SS bands between conformers, with A having a stronger non-H-bonded band (2845 cm^{-1}) and B a stronger H-bonded band (2853 cm^{-1}). In what follows, we exploit this difference in assessing the presence of *syn/anti* conformational pairs. The mid-IR region is quite complex, especially below 1400 cm^{-1} where CH bend, OH bend, and C–O stretch fundamentals arise. At higher wavenumber, the C=O stretch and C=C stretch bands are readily assigned.

The calculated IR spectra for the structures assigned to A and B are shown below the experimental spectra in Figure 5. Between conformers A and B, the simulated spectra are very similar, but the overall fit to experiment is relatively good. The calculation predicts a 6 cm^{-1} splitting between the free

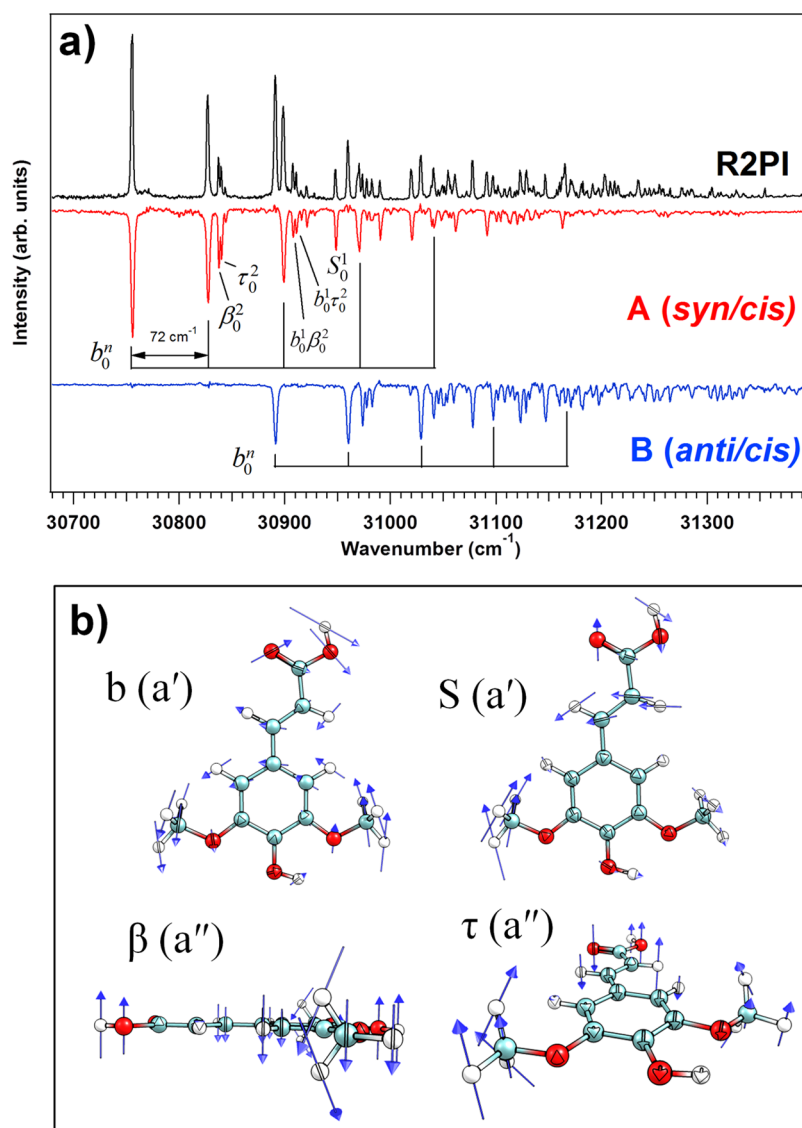


Figure 3. (a) R2PI spectrum (black) and UV–UV HB spectra of conformers A (red) and B (blue) for SA. UV–UV HB was taken by fixing the holeburn laser on the origin transitions of conformers A and B. (b) Franck–Condon active vibrations in sinapic acid: *b*, C₄–C₇=C₈ bend; *S*, C₇=C₈–C₉(O) scissor; *β*, butterfly; *τ*, C₄C₇ torsion/symmetric methoxy torsion. Refer to Figure 1a for atom numbering.

carboxylic acid OH and syringyl OH fundamentals of the planar structures, but these bands are not resolved in the spectrum. The calculated spectra in the 1500–1800 cm⁻¹ region match the experimental spectra well, validating the assignment of the bands at 1766, 1656, and 1627 cm⁻¹ to C=O stretch, C=C_{vinyl} stretch, and C=C_{ar} stretch fundamentals, respectively.

While only slight differences are observed between the two conformers in the IR, further verification of the appropriate *syn/anti* assignments can be found in the electronic origin splitting. Vertical excitation energy calculations at the TDDFT//M05-2X/6-31+G(d) level of theory predict the *syn* conformer red of the *anti* conformer, and when scaled to the origin transition of conformer A (scale factor = 0.9038), the calculated splitting is 168 cm⁻¹. As a result, we tentatively assign conformer A to the *syn/cis* conformer and B to *anti/cis*. The experimental and calculated origin frequencies for conformers A and B can be found in Table 1. Interconversion between *syn* and *anti* minima of the *cis* (planar) conformational family (assigned to conformers A and B) can occur by hindered rotation about the C₃C₄C₇C₈ dihedral. To estimate the barrier

between these two conformers along this coordinate, a relaxed potential energy scan was carried out and is shown in the Supporting Information; the barrier height is predicted to be 24 kJ/mol (2006 cm⁻¹), and the second pathway to interconversion by rotation about the C–O(H) bond yields a slightly higher barrier at 26.8 kJ/mol (2240 cm⁻¹).

3.2. Methyl Sinapate (MS) and Isopropyl Sinapate (IS) Spectroscopy. 3.2.1. R2PI and UV–UV HB Spectroscopy.

The simplest extension from sinapic acid to its ester derivatives is to replace the carboxylic acid hydrogen with a methyl group, forming the methyl ester, methyl sinapate (MS). The R2PI and UV–UV HB spectra for MS are shown in Figure 6a. This substitution shifts the electronic origin to the blue by 309 cm⁻¹, a surprisingly large amount given how remote this substitution is from the aromatic ring. However, since the electronic conjugation extends to the end of the molecule, methyl substitution does play a role in inducing an electronic frequency shift, and is consistent with the large geometry change in the vinyl-containing substituent. Three conformers were found in methyl sinapate, two of which dominate the population, and the

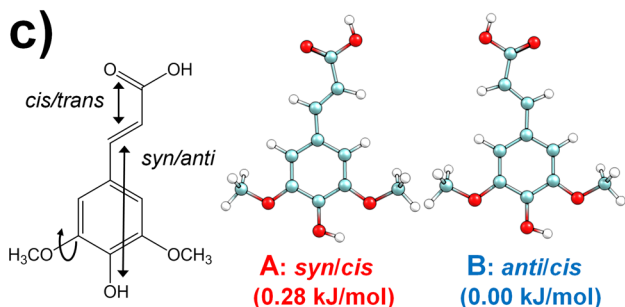
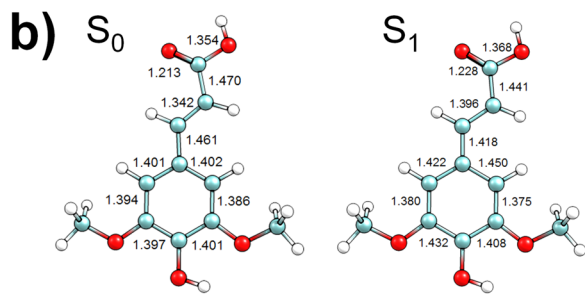
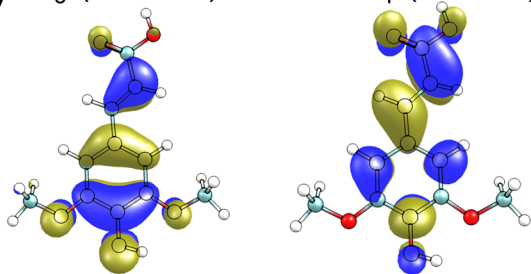
a) S_0 (HOMO) \longrightarrow S_1 (LUMO)

Figure 4. (a) Molecular orbitals for the $S_0 \rightarrow S_1$ transition in SA and (b) optimized bond distances (Å) for S_0 and S_1 structures calculated at the TDDFT//M05-2X/6-31+G(d) level of theory. (c) Conformational degrees of freedom in SA (left) and assigned structures for conformers A and B in SA.

third a very minor conformer just barely observed. Once again, for the two major conformers, long progressions are found with frequencies of 59 and 57 cm^{-1} for A and B, respectively,

Table 1. Assignments, Zero-Point Corrected Energies, and Experimental and Calculated Origin Frequencies for the Observed Conformers in the Sinapate Series

conformer	assignment	E^a (kJ/mol)	origin ^{exp} (cm^{-1})	origin ^{calc} (cm^{-1}) ^{a,b}
SA (A)	<i>syn/cis</i>	0.28	30756	30755
SA (B)	<i>anti/cis</i>	0	30891	30918
MS (A)	<i>syn/cis</i>	0.3	31065	31023
MS (B)	<i>anti/cis</i>	0	31174	31175
MS (C)	<i>anti/trans</i>	4.26	31285	31341
IS (A)	<i>syn/cis</i>	0.09	31046	31051
IS (B)	<i>anti/cis</i>	0	31157	31193
SML (A)	<i>syn/cis</i>	0	30713	30225
SML (B)	<i>anti/cis</i>	0.35	30847	30364
SMB (A)	<i>syn/cis</i>	0	30737	30016
SMB (B)	<i>anti/cis</i>	0.46	30924	30203
SM	<i>syn/cis</i>	0		29646
SM	<i>anti/cis</i>	0.61		29845
SDM	<i>syn/cis</i>	0		29813
SDM	<i>anti/cis</i>	0.58		30005

^aDFT//M05-2X/6-31+G(d). ^bScaled by 0.9038.

extending up to seven quanta in conformer A. This band is assigned to the same bending mode (b_{00}^b), and the frequency is decreased from sinapic acid due to the heavier methyl group at the terminus. The splitting between the origins of conformers A and B is 109 cm^{-1} , an amount similar to that in SA. On the basis of the assignments for SA, we tentatively assign the red-shifted A conformer of methyl sinapate to the *syn* conformer and the blue-shifted B conformer to its *anti* counterpart. The two are calculated to be within 0.30 kJ/mol of one another, with *anti/cis* below *syn/cis*. Interestingly, the *syn/cis* conformer displays a longer Franck–Condon progression in the vinyl bend b , the opposite of that found in sinapic acid.

The other low-frequency bands at 72 (73) and 76 (79) cm^{-1} in conformer A (B) are assigned to β_0^2 and τ_0^2 transitions, showing that these conformers still obey C_s selection rules, proving that both ground and S_1 excited states of both molecules are planar. $b_1^1\beta_0^2$ and $b_1^1\tau_0^2$ combination bands appear just blue of b_0^2 , and the S_1^0 fundamental emerges at +161 cm^{-1} . The electronic origin of conformer C is blue-shifted from both major conformers, appearing at 31285 cm^{-1} .

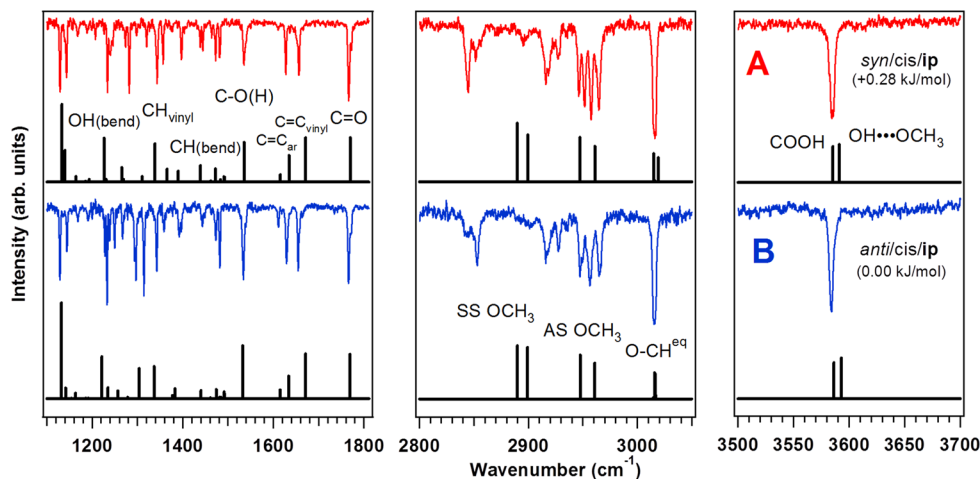


Figure 5. RIDIR spectra for conformers A (top, red) and B (bottom, blue) of SA in the OH stretch (right), alkyl CH stretch (middle), and mid-IR (left) regions with calculated stick spectra below each experimental spectrum, calculated at the DFT//M05-2X/6-31+G(d) level of theory.

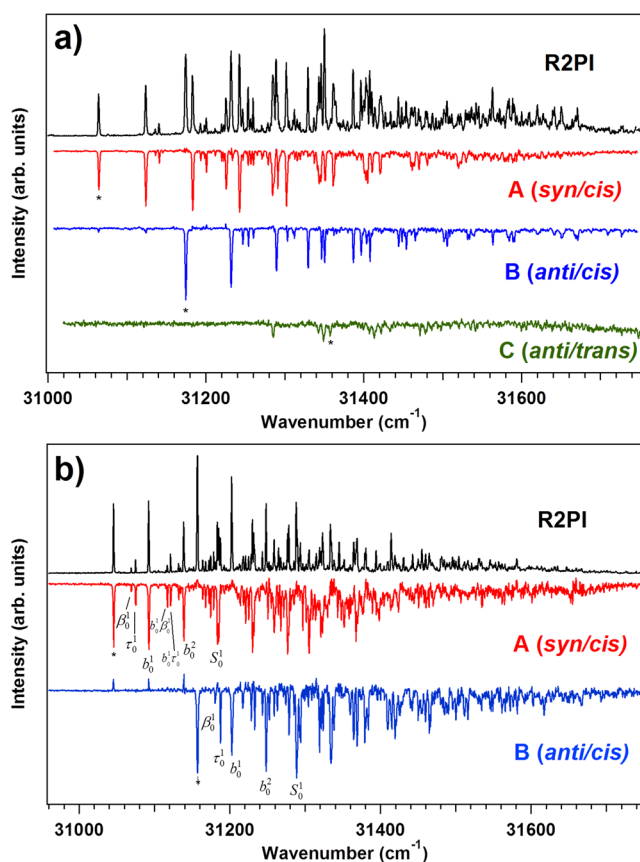


Figure 6. R2PI spectrum (black) and UV–UV HB spectra of (a) conformers A (red), B (blue), and C (green) of MS and (b) conformers A (red) and B (blue) of IS. Asterisks indicate transitions used for UV–UV HB.

Calculated vertical excitation energies place the *syn/cis* conformer furthest to the red among all calculated conformers, with the *anti/cis* predicted at $+152\text{ cm}^{-1}$ and the *anti/trans* at $+318\text{ cm}^{-1}$. Similar splittings between *cis* and *trans* conformers were observed experimentally for *p*-coumaric acid and its methyl ester.^{21,22} On this basis, conformer C is tentatively assigned to the *anti/trans* conformation, calculated to have an energy of 4.26 kJ/mol above the global minimum. The experimental and calculated origins can be found in Table 1.

As a next step in building up the full complexity of the sinapoyl malate side chain, an isopropyl group was substituted in place of the methyl group in MS, forming isopropyl sinapate. Notably, the isopropyl group also breaks the planar symmetry, yet without introducing additional functional groups to the molecule. The R2PI and UV–UV HB spectra for isopropyl sinapate (IS) reveal spectra that are resolved but quite congested, as shown in Figure 6b. As with SA and MS, just two major conformers were observed, with S_0 – S_1 origin transitions split by 111 cm^{-1} , only 2 cm^{-1} larger than in methyl sinapate; therefore, the two nearly equally abundant conformers are assigned as the *syn/anti* pair of the *cis* C=C/C=O family, as in SA and MS. Once again, it is possible to assign the low-frequency vibronic structure, with excellent agreement between experiment and calculated frequencies for the excited state vibrations (Table S1, Supporting Information). In breaking the mirror symmetry through the chromophore plane with the isopropyl group, a'' fundamentals are allowed and observed just above the origin transition, as labeled in Figure 6b. Indeed,

according to calculation, the isopropyl group asymmetrically staggers the chromophore plane, placing one methyl group $+80^\circ$ and the other -22° from the plane. It should be noted that, among the calculated structures, degenerate pairs were found for structures that oriented the isopropyl group in the identical configuration except on opposite sides of the plane, i.e., $\text{CH}_3^a(80^\circ)/\text{CH}_3^b(-22^\circ)$ and $\text{CH}_3^a(22^\circ)/\text{CH}_3^b(-80^\circ)$. These structures are identical and indistinguishable in the UV spectrum.

3.2.2. Fluorescence Spectroscopy of Methyl Sinapate. LIF and DFL spectroscopy was carried out on MS for measurement of the fluorescence lifetime and a qualitative check on the fluorescence quantum yield. The fluorescence lifetimes of the electronic origins of conformers A and B of MS were approximately 12 and 14 ns, respectively. We surmise that no fast nonradiative processes are at play in the simple case of MS, based on its relatively long fluorescence decay and large fluorescence signal.

The DFL spectra of the origin transitions of conformers A and B are shown in parts a and b of Figure 7, respectively. As in

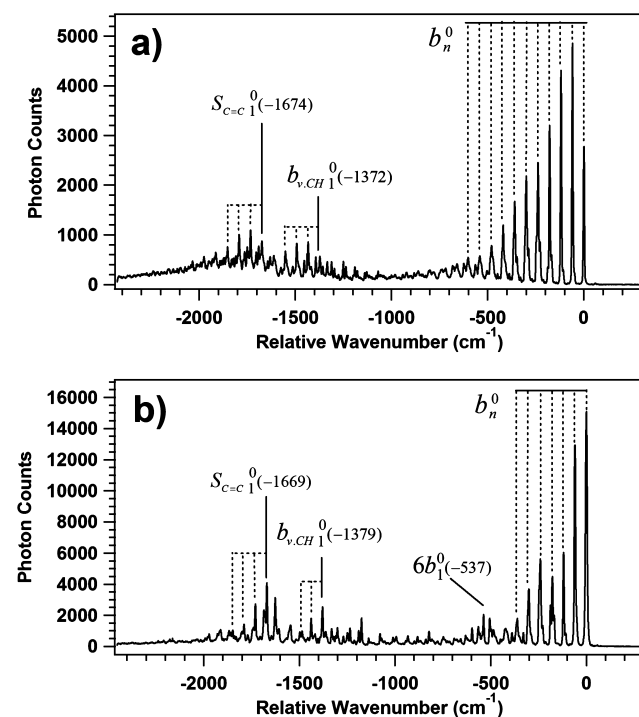


Figure 7. DFL spectra of the S_1 origin transitions of conformers A (a) and B (b) of MS.

the UV excitation spectra, long Franck–Condon progressions involving the C_4 – C_7 – C_8 bend are observed, with the pure b_n^0 progression extending out to ten quanta in conformer A and potentially six in B. These bands dominate the spectra in Figure 7, hindering detection of the weak β and τ overtone transitions. The ground state frequency of the bending mode for both conformers is 59 cm^{-1} , effectively unchanged from the excited state. Franck–Condon analysis of the b_n^0 progression in the DFL spectrum of conformers A and B (Figure 7) yielded displacement parameters of approximately $D = 2.0$ and 1.3 , respectively.³⁷ Transitions to high “ n ” levels in the ground state have intensities that likely have unresolved contributions from a second fundamental, distorting the intensities of these bands.

The vinyl CH bend fundamental, $b_{\nu, \text{CH}}^0$, and the C=C stretch fundamental, $S_{\text{C}=\text{C}}^0$, are also prominent in the spectra, with b_n^0 progressions built off of them, as highlighted in Figure 7. The strong Franck–Condon factors for these modes are in accord with the proposed geometry change associated with the S_0 – S_1 electronic transition, favoring those modes that correspond to changes in the single and double bond character of the $-\text{C}=\text{C}-\text{C}=\text{O}$ substituent associated with the $\pi\pi^*$ transition.

3.3. Sinapoyl Methyl-Lactate (SML) and Sinapoyl Methyl-Butyrate (SMB) Spectroscopy. The studies detailed in the previous sections on sinapic acid, methyl sinapate, and isopropyl sinapate have provided a sound basis for extension to sinapoyl malate-like molecules. As shown in Figure 2, sinapoyl malate itself possesses a structureless R2PI spectrum that represents a fascinating, seemingly cataclysmic change in the excited state spectroscopy and/or dynamics. Therefore, to search for an onset of such behavior, sinapate ester derivatives containing only one-half of the dicarboxylate malate side chain were synthesized and studied. The malate side chain has its two carboxylic acid groups separated from the ester oxygen by one and two carbons, respectively. Given that both the dicarboxylic acid and methyl dicarboxylate SM molecules yielded broadened UV spectra (Figure 2), we chose to study the methyl carboxylate derivatives of the separate malate “halves”. In addition, a methyl group was used at the other end of the side chain (C_{11} or C_{12}) to better mimic the conformational aspects of malate by preventing artificial flexibility of the single side chain (see Figure 1), forming sinapoyl methyl-lactate (SML) and sinapoyl methyl-butyrate (SMB), with structures shown in Figure 1a.

3.3.1. R2PI and UV–UV HB Spectroscopy. The 2C-R2PI and UV–UV HB spectra of SML are shown in Figure 8a. The R2PI spectrum still shows well-resolved vibronic structure, and an appearance similar to that of its smaller counterparts, but the spectrum also shows signs of additional congestion/broadening. UV–UV HB spectroscopy once again identifies the presence of two conformational isomers. The S_0 – S_1 origin for conformer A appears at 30713 cm^{-1} , now shifted back to the red closer to those of SA and SM. Although the UV–UV HB spectrum of conformer B clearly contains contributions from A due to spectral overlap, the large discrepancy in intensities between A and B transitions and the diagnostic b-progressions allows for clear identification of transitions due to conformer B. The characteristic splitting between the electronic origins (134 cm^{-1}) and Franck–Condon activity attributed to these conformers points clearly to their assignment as the *syn/cis* (A) and *anti/cis* (B) conformers, respectively. Computational predictions also verify this assignment, with the *syn/cis* conformer calculated as the global minimum, and its *anti* counterpart only $+0.35 \text{ kJ/mol}$ higher in energy.

The increased side chain flexibility in SML produces additional low-energy conformational minima associated with side chain reorientation, predominantly defined by the $C_9\text{OC}_{10}C_{11}$ dihedral, which positions the $C_{11}=\text{O}$ either *cis* or *trans* to the ester oxygen between C_9 and C_{10} . The low energy structures nominally incorporate a *trans* $C_{11}=\text{O}$ configuration, while analogous structures that incorporate the *cis* configuration begin $\sim 7 \text{ kJ/mol}$ higher in energy. Conformers A and B of SML are tentatively assigned to the global minimum side chain conformation, with structures shown in detail in the Supporting Information.

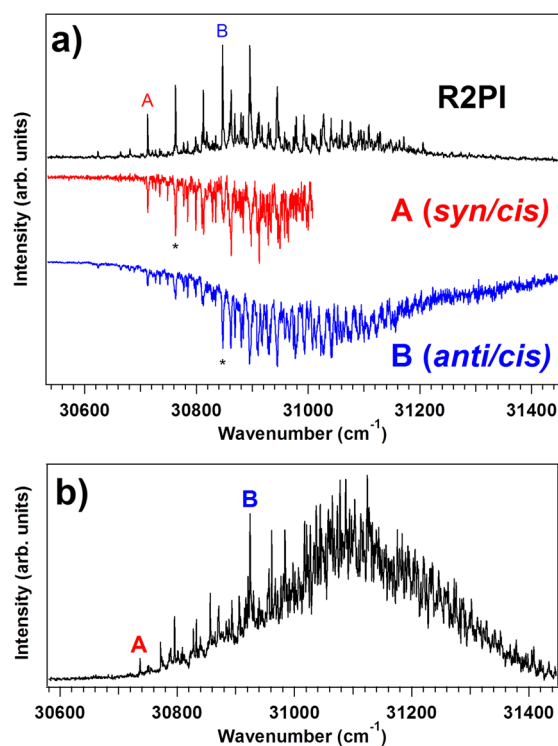


Figure 8. (a) 2C-R2PI spectrum (black) and UV–UV HB spectra for conformers A (red) and B (blue) of sinapoyl methyl-lactate (SML) and (b) 2C-R2PI of sinapoyl methyl-butyrate (SMB). Asterisks indicate UV–UV HB transitions. Bands to the red of the B origin in part a are due to spectral overlap at the UV holeburn transition.

One notable aspect of the UV absorption of SML compared with the other compounds was its extreme sensitivity to photon fluence. To properly record an R2PI spectrum without marked saturation effects, 2C-R2PI was required with excitation laser powers as low as $4\text{--}10 \mu\text{J/pulse}$ ($\Phi \sim 0.4 \text{ mJ/cm}^2$), versus typical excitation powers of $\sim 30\text{--}100 \mu\text{J/pulse}$ for 1C-R2PI used for the simpler sinapates. The implications of this fact will be discussed further in the Discussion section.

Fluorescence spectroscopy was also performed on SML, and it was found that the total fluorescence signal compared to methyl sinapate was only slightly less, but the lifetime was noticeably shorter, with an instrument-limited response providing an upper bound of 8 ns to its S_1 lifetime. The DFL spectra of the conformer A and B origin transitions were acquired and can be found in the Supporting Information. While the total fluorescence signal for SML was $\sim 10\%$ of that of MS, transitions in the Franck–Condon region of the DFL spectrum were $<1\%$ the size. This suggests that much of the “missing” emission intensity is shifted well to the red, out of the Franck–Condon window. Such Stokes-shifted emission is quite common when coupling of the locally excited $\pi\pi^*$ state to a second excited state (e.g., a charge-transfer state) occurs.^{38–40} Dispersed emission was also collected over 50 nm for conformer B, but no red-shifted emission was detected.

Because detection of broadened, red-shifted emission could be difficult in DFL spectra, a series of excitation spectra were recorded with short wavelength cutoff filters (345, 400, and 425 nm) in front of the PMT detector, to test whether a second contribution to the absorption profile might be buried underneath the sharp transitions. A monotonic decrease in

fluorescence signal was observed for all transitions, with no evidence of dual excitation profiles found.

The derivative incorporating the longer “half” of the malate side chain is sinapoyl methyl-butyrate (SMB) shown in Figure 1b. This molecule has one more carbon along its side chain introducing an additional element of flexibility. The 2C-R2PI spectrum for SMB taken under the same low-fluence conditions as SML is shown in Figure 8b. While sharp transitions are clearly discernible, they are built off of a large background that by appearances represents an intermediate case between sinapoyl methyl-lactate and sinapoyl malate. UV–UV HB spectra were not obtained for SMB due to low signal levels and lack of band isolation. If the first band is taken as the first origin transition (A), tentatively assigned to a *syn/cis* conformer, a progression can be followed for at least two quanta, suggesting a ν_b' frequency of 59 cm^{-1} . While this is surprisingly larger in frequency than in SML, a comparison of the calculated frequencies between these molecules supports this assignment. Other bands built off of this origin are found at +15 and +35 cm^{-1} similar to those low frequency modes in SML. Given the relative intensities and splittings between the *syn* and *anti* conformers of the molecules presented up to this point, inspection of the SMB R2PI spectrum leads to a tentative assignment of the *anti/cis* origin at 30924 cm^{-1} , 187 cm^{-1} blue of the A origin. From this origin, there are prominent +37 and +59 cm^{-1} bands presumed to be analogous features to those found built off of conformer A.

It is possible that other conformers are present within the spectrum, and calculations predict seven conformers within 5 kJ/mol, with four more structures in this low energy window than in SML. We must rely on calculations for assignment of the side chain conformation for the *syn/cis* and *anti/cis* conformers assigned in the spectrum, and those conformational details are given in the Supporting Information.

3.4. Sinapoyl Malate (SM) and Sinapoyl Dimethyl Malate (SDM) Spectroscopy. **3.4.1. R2PI Spectroscopy.** By evaluating the vibronic spectroscopy of sinapic acid and its ester derivatives, and determining the common conformational distribution among this class of molecules, the spectroscopy of the biologically relevant sinapoyl malate can be addressed. The R2PI spectra for SM and its dimethyl carboxylate derivative SDM are shown in Figure 9. As noted from Figure 2, both of these spectra are broadened, and seemingly featureless. The UV absorption of these molecules begins at $\sim 30500\text{ cm}^{-1}$, further red than any of the ester derivatives analyzed up to this point. The spectral profile is asymmetric, with the SM spectrum peaking near 30700 cm^{-1} and extending past 31200 cm^{-1} with a gradual decay to the blue. SDM was investigated in order to ensure that the broadening observed in the UV was not resulting from the acid COOH groups in SM alone. The R2PI spectrum of SDM is nearly identical to SM, and it incidentally provided a test case for laser fluence studies due to a higher signal-to-noise ratio (S/N) for its R2PI spectrum and therefore a higher sensitivity to spectral features. As a result, the spectrum for SDM was recorded over a wider wavelength range ($>1200\text{ cm}^{-1}$), revealing an absorption extending past 31700 cm^{-1} . While it appears that some remnant band structure might be present in the sinapoyl malate spectrum, none were reliably reproducible, and the higher S/N spectrum of SDM yielded no sign of reproducible structure, even near the onset of its spectrum where the density of S_1 states is lowest. 2C-R2PI was performed on SDM with the low-fluence conditions used for SML and SMB, to firmly determine

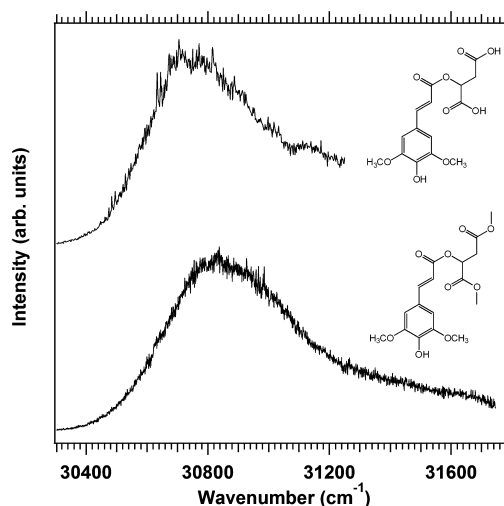


Figure 9. R2PI spectra for sinapoyl malate, SM (top), and sinapoyl dimethyl malate, SDM (bottom).

whether the broadening in the SM/SDM spectra was inherent to the molecules and not strictly due to a high absorption coefficient inducing saturation effects. No reproducible structure was found.

3.4.2. Computational Predictions of Conformational Families. The sinapoyl malate structure incorporates the full malate side chain introducing a larger variety of conformational families available to it. The global minimum *syn/cis* structure calculated for sinapoyl malate is shown in Figure 10a. For the

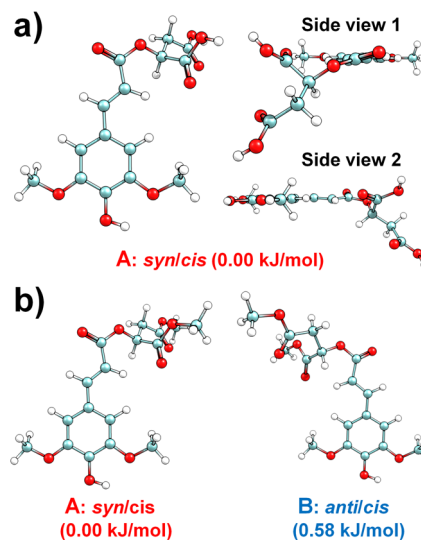


Figure 10. Calculated structure for the global minimum conformation of (a) SM, with top and side views (right), and (b) the lowest energy structures found for SDM.

lowest-energy *syn/cis* and *anti/cis* structures, the syringyl methoxy groups are planar with the aromatic ring. The longer alkyl chain ($C_{10}C_{12}C_{13}$) is extended in a nominally planar configuration ($C_{10}C_{12}C_{13}OH$ plane), with the first carboxylic acid group ($C_{11}OOH$) oriented perpendicular to the aromatic ring. The extended $C_{10}C_{12}C_{13}OH$ part of the side chain is approximately 20° below the plane of the sinapate itself (side view of Figure 10a). Interestingly, the bulky size of the malate group prevents the close approach of either of the carboxylic

acid groups to the sinapate moiety, unlike the case of SML and SMB. For the lowest two structures with this malate conformation, the C=O groups are still nominally pointing back toward the aromatic ring (Figure 10a), as was the case for the SML and SMB conformations (Supporting Information). All of the oxygen-containing groups are well over 3 Å from one another due to the steric constraints, prohibiting the formation of any intramolecular H-bonds.

Within 10 kJ/mol of the global minimum, a total of 28 conformational minima were found, differing by their malate conformation, HO/C=C configuration (*syn/anti*), and degree of planarity of the non-H-bonded methoxy group on the ring. Approximately half of those 28 structures incorporated the planar syringyl ring, with no experimental evidence for the nonplanar syringyl conformation in any of the sinapate esters.^{41,42} No C=C/C=O *trans* conformers were found within this 10 kJ/mol window. The next set of side chain structures incorporating the all-planar syringyl ring are found at 2.36, 5.82, and 6.11 kJ/mol above the global minimum, and they differ primarily by their malate dihedral angles summarized in Table 2. A detailed description of these calculated structures can be found in the Supporting Information.

Table 2. Relevant Dihedrals for Different SM Side Chain Conformations from DFT//M05-2X/6-31+G(d) Structural Optimizations

E (kJ/mol)	C ₉ OC ₁₀ C ₁₁	OC ₁₀ C ₁₁ =O	OC ₁₀ C ₁₂ C ₁₃	C ₁₀ C ₁₂ C ₁₃ =O
0	-93.7	95.1	177	-2.37
2.60	-82.2	-174	65.5	25
5.82	50.6	-137	-161	23.6
6.11	-59	145	-177	-118

The broad, featureless UV spectra of the sinapoyl malate molecules SM and SDM prevent the acquisition of conformation-specific IR data. However, composite IR spectra were taken by monitoring the depletion of ion signal generated from UV excitation at the peak of the broad UV absorption (~ 30700 cm⁻¹ in SM). The IR spectra of SM and SDM in the OH stretch (SM), alkyl CH stretch, and mid-IR regions, along with detailed spectral analysis, are given in the Supporting Information. The OH stretch fundamentals of the CO–OH groups are not resolved but appear as a single band in the free COOH OH stretch region, as anticipated on the basis of the low-energy structures, due to their inability to engage in hydrogen bonds or interact with the sinapate aromatic ring. The IR spectra of SM and SDM could not be used to make a firm conformational assignment; however, some features of the spectrum are worth noting. First, the sharp (~ 4 cm⁻¹ fwhm), well-resolved IR transitions prove that the probed molecules are indeed rotationally cold, so that the observed broadening is not simply a thermal effect. Second, using the IR spectra of conformers A and B of sinapic acid (Figure 5) as a reference, particularly in the CH stretch region, the relative intensities of absorptions specific to *syn* and *anti* rotamers were nearly equally represented in the SM composite spectrum. Furthermore, RIDIR spectra taken at multiple UV probe wavelengths (across the SM absorption) were identical, indicating that the conformers contributing to the spectrum contribute equally across the UV absorption profile.

On the basis of this data and our experience with other members of the series, we surmise that the population in the expansion consists either primarily or exclusively of the same

syn/anti pair of conformers as were present in the simpler sinapate esters, here employing the most stable malate conformation in both, in nearly equal abundance. The calculations are used to tentatively determine the specific malate conformation, shown in Figure 10, relying on the fact that the employed computational methods have accurately predicted the same pair of conformations to be present in other members of the series so far considered, providing evidence of its predictive capability for SM and SDM.

4. DISCUSSION

As the key UV-B screening agent in many plants, sinapoyl malate and related sinapate esters are vital to the survival of plants. Nature's selection of the sinapate esters for this purpose is evident in their unique properties as UV-B absorbants. First, the sinapate esters as a family all possess strong S₀–S₁ UV absorptions that peak in the UV-B region, with oscillator strengths “*f*” for their S₀–S₁ transitions approaching 1. Thus, the per-molecule absorption strength is as efficient as possible, as one might expect for a UV-B sunscreen. Second, of the members of the series, sinapoyl malate is itself quite unique in having an inherently broadened UV absorption that gives near-complete wavelength coverage even under jet-cooled, isolated-molecule conditions. The question is why. In what follows, the characteristics of the sinapate S₀–S₁ excitation and potential mechanisms to account for the broadening in SM will be explored. Having considered these mechanisms, we will return to consider the potential implications that this broadening might have for SM as a sunscreen for plants.

4.1. Nature of the Sinapate Electronic Excitation. The characteristics of the π – π^* transition responsible for the high sinapate absorbance in the UV-B spectral region were briefly discussed in section 3.1 for sinapic acid. According to the TDDFT calculations, the HOMO \rightarrow LUMO transition is the prominent contributor to the electronic transition in all of the sinapates presented in this work, and the MOs shown for SA in Figure 4a are representative for the excitation in the entire series. The characteristic geometry change that accompanies this excitation is reflected in the long Franck–Condon progressions involving the C₄–C₇=C₈ bend vibration.

p-Coumaric acid (pCA) and methyl 4-hydroxycinnamate (MeOpCA) are close analogues of the prototypical members of our sinapate ester series, sinapic acid and methyl sinapate, lacking only the methoxy groups in the two *ortho* positions on the ring. The electronic spectroscopy of pCA and MeOpCA has been thoroughly investigated both experimentally^{21–24} and computationally,⁴³ and provides a basis for comparison with the sinapate esters. In both pCA and MeOpCA, three relevant singlet states were calculated, corresponding to the HOMO \rightarrow LUMO $\pi\pi^*$ state discussed here (denoted “V” for “valence”), a second $\pi\pi^*$ of primarily HOMO \rightarrow LUMO+1 character (denoted “V'”), and a HOMO–3 n-type orbital \rightarrow LUMO $n\pi^*$ state associated with the nonbonding orbital on the C=O oxygen.^{21,22,43} These states are differentiated by their MO character but also the oscillator strengths for the S₀ \rightarrow S_n transition. Calculations for pCA and MeOpCA predicted a large oscillator strength for transitions from the ground state to the V state (~ 0.65 – 0.7), and ~ 0.02 – 0.18 for the V' state.^{21,22,43} In pCA and MeOpCA, the S₁ state was found to be the V' state, which possessed only weak Franck–Condon activity in the b-mode, and dominating $\Delta\nu = 0$ Franck–Condon factors. The same state ordering was presumed in the

cinnamates MMC and EHMC, where similar excited state lifetimes and absorption frequencies were observed.²⁰

In sinapic acid and methyl sinapate, the V/V' states show similar characteristics. The Franck–Condon simulations for the V and V' excitations are shown for the *syn/cis* conformer of SA in the Supporting Information as an example. The simulation unambiguously verifies the assignment of the S₁ state in sinapate chromophores as the V ($\pi\pi^*$) state, which has a very large oscillator strength and long FC progressions in the β mode.

The S₀–S₁ absorption of pCA, MeOpCA, MMC, and EHMC is centered around 33000 cm⁻¹, over 2000 cm⁻¹ above the sinapate absorption. Thus, the two methoxy groups present in the sinapates shift conjugation out onto the methoxy groups, adding to the electronic delocalization, and lowering the V state relative to V', thereby switching the order of the S₁/S₂ states. TDDFT calculations for pCA and MeOpCA falsely predict the V state at lower energy than V'; however, this same ordering was calculated for the sinapate molecules of interest here, and in this case is in keeping with experiment. The TDDFT//M05-2X/6-31+G(d) unscaled vertical excitation energies for the first three singlet states are summarized in Table S2 in the Supporting Information for the assigned conformers in the sinapate series. The same V ($\pi\pi^*$), V' ($\pi\pi^*$), and $n\pi^*$ states are present in the sinapates, and the calculated V–V' separation is approximately equal to that calculated for pCA/MeOpCA with TDDFT.²¹ To illustrate the electronic transitions associated with each of these three excited states, the calculated MOs comprising the primary electronic transition for each of these ground to excited state transitions are shown in Figure 11a, b, and c for SM.

The bright S₀–V $\pi\pi^*$ transition in sinapoyl malate (Figure 11a) promotes an electron from a π HOMO that possesses C₄–C₇=C₈–C₉=O (single–double–single–double) bond character to a π^* LUMO with C₄=C₇–C₈=C₉–O bond character. It should be noted that the electron density in the LUMO has little contribution on the malate side chain. The second $\pi\pi^*$ state (V') which was not observed in this experiment is attributed mostly to the HOMO–1 → LUMO transition shown in Figure 11b, which yields a smaller absorption coefficient, with electron density localized on the aromatic ring in HOMO–1. The primary configuration for the $n\pi^*$ state is of interest, as the anticipated localization to the nominally assigned nonbonding orbital on the C₉=O (as in SA) is lost to some degree in sinapoyl malate, with electron density extending all the way out into the first carboxylic acid of the malate moiety. This delocalization makes it a peculiar “non-bonding” MO, differing significantly from simpler systems that do not contain the malate group, such as sinapic acid.

As Table S2 (Supporting Information) shows, TDDFT calculations predict no major changes to the vertical energy separations between the S₁, S₂, and S₃ states along the series of molecules, with the V state always well below the others. Furthermore, the direction and magnitude of the shift in the vertical S₀–S₁ transition along the series SA, MS, IS, SML, and SMB are in qualitative agreement with the experimental electronic frequency shifts (Table S2, Supporting Information, c.f. Table 1). The calculations also faithfully reproduce the experimental splitting between *syn* and *anti* OH/C=C orientations, which are not modified significantly along the series, with *syn/cis* below *anti/cis* by about 200 cm⁻¹.

At the same time, the calculated S₀–S₁ vertical splittings between the *syn/cis* and *anti/cis* conformers of the sinapate

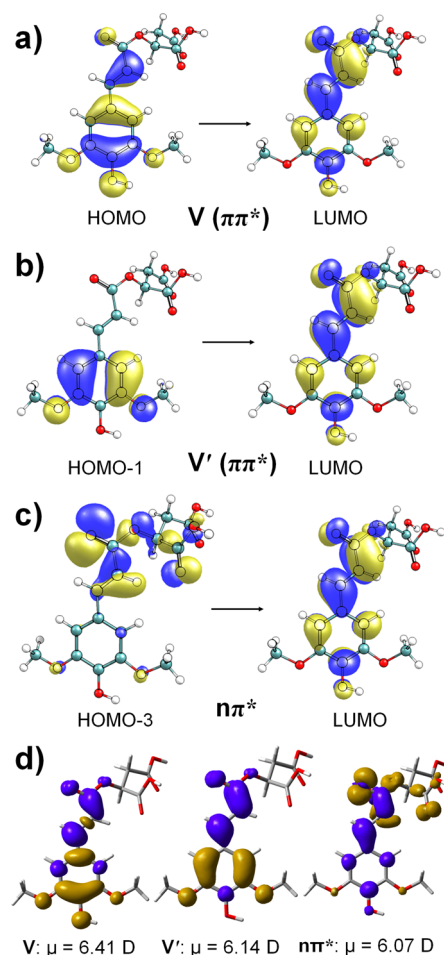


Figure 11. Molecular orbitals for the three relevant singlet state excitations in sinapoyl malate: (a) V ($\pi\pi^*$), (b) V' ($\pi\pi^*$), and (c) $n\pi^*$. (d) Electron density difference maps (EDDMs) of the three singlet excited states of SM. Blue represents a gain in electron density, while yellow represents a loss.

esters containing carboxylates/carboxylic acids (SML, SMB, SM, and SDM) are calculated to be further to the red than the experimental spectra would suggest they should be. This is either indicative of a larger geometry change or of deficiencies in the TDDFT calculations in these cases in which the COOX groups on the side chain are near the chromophore. The scaled excited state energies and relative oscillator strengths for the assigned conformers are plotted along with the experimental R2PI spectra in the Supporting Information (Figure S8), further illustrating this fact.

The assignment of the S₀–S₁ UV-B excitation to the bright V ($\pi\pi^*$) state is unequivocal, and validated through experiment and calculations. The oscillator strength of this transition in sinapoyl malate is calculated to be ~ 0.65 , confirming its status as an efficient absorber of UV-B radiation. Besides this efficiency as an absorber, the absorption strength is spread out over much of the UV-B region due to strong Franck–Condon activity involving low-frequency in-plane and high-frequency bond stretching coordinates associated with the change in double-bond/single-bond character accompanying excitation to the V state. It is for this reason that the V state in pCA has been postulated to mediate *trans*–*cis* photoisomerization about the C₇–C₈ bond.^{24,43} In addition, the Franck–Condon active low-frequency out-of-plane butterfly, β , and

torsional, τ , modes serve to congest the S_0 – S_1 absorption through combination bands with intense b_0^n transitions. The activity in these modes is a characteristic feature of the sinapate chromophore, proven by the extent of their activity in every molecule studied here. The vibronic congestion brought about by these active low-frequency modes is manifested in the gas phase UV spectra, particularly with molecules incorporating a large side chain, which drops the frequency of the β and τ fundamentals to as low as 10 cm^{-1} . Coupled to this vibronic activity is the “doubling” of transitions due to the population of the *syn/anti* rotamers in nearly equal abundance. The small frequency shift of the S_0 – S_1 absorptions of these conformers ($\sim 150\text{ cm}^{-1}$) spreads out the inherent vibronic activity even further and congests the total excitation spectrum.

4.2. Mechanism for Broadening in Sinapoyl Malate.

The S_0 – S_1 R2PI spectra of sinapoyl malate and its dimethyl derivative, SDM, display a broad featureless absorption, which sets it apart from the simpler derivatives studied in this work. While this broadening prohibits vibronic analysis, its manifestation points to aspects of the excited states of sinapoyl malate that are unique (in this series), and may actively play a role in the selection of sinapoyl malate as a UV-B protectant in plants. The trends recognized from the UV spectroscopy of the sinapate ester series studied here, along with the UV and IR spectroscopy of SM/SDM itself, provide a basis on which to evaluate the possible mechanisms giving rise to the inherent broadening in SM.

4.2.1. Vibronic Congestion. One circumstance to be considered is one already alluded to in evaluating the SA–SM series: inherent vibronic congestion. One clear trend in the series presented here is the level of congestion brought on by low-frequency modes, coupled with the extensive activity of the b -mode (Figure 3b). The malate side chain presents the largest reduced mass in the series, resulting in the lowest frequencies for the set of active vibrations sensitive to the electronic absorption. The sinapate chromophore itself is inherently sensitive to these large amplitude vibrations due to the nature of the S_0 – V transition, which extends out to the site of substitution of the malate side chain (Figure 11a). While a simple increase in congestion is undoubtedly a contribution to the broad and extended absorption of SM, it is unlikely that this alone would lead to a complete washing out of all sharp structure even at low frequency near the electronic origin, where the S_1 vibrational state density is lowest. For instance, even in SMB where the spectral broadening first becomes apparent, vibronic analysis can still be accomplished up to the b_0^1 band.

In addition to vibronic congestion, however, intramolecular vibrational redistribution (IVR) could also contribute as a mechanism for vibronic congestion/broadening. While the number of low-frequency modes (which provide the predominant contribution to the bath for IVR) does increase along the sinapate ester series, the increase is actually quite modest, with the isopropyl sinapate/sinapoyl methyl lactate/sinapoyl malate series possessing seven/eight/nine modes, respectively, with frequencies below 100 cm^{-1} . Furthermore, the decrease in frequency of these modes with increasing size of the side chain is also quite small. Sinapoyl methyl-lactate (SML) provides a testing ground for the effects of IVR in S_1 , since the spectrum is still resolvable, yet dense. Indeed, some apparent band broadening is observed beginning about 200 – 300 cm^{-1} above the conformer A origin transition; however, this is attributed more to spectral overlap than from IVR. As such, it is

not expected that IVR should play a dominant role in the excited state of sinapoyl malate near its origin, as it appears to have minimal effect on the closely related analogue SML, where sharp structure is readily observed near the electronic origin.

A related possibility is that the Franck–Condon region in sinapoyl malate begins well above the electronic origin where the S_1 density of states is very high, thereby preventing resolution of individual transitions. While this idea is in line with TDDFT calculations which predict a red-shift of larger magnitude for the onset of the electronic transition in SM, the electronic origins of the two conformers of SML are clearly observed, and indicate that the TDDFT calculations overestimate the calculated electronic frequency shifts of the malate-containing derivatives. Furthermore, structural optimization of the S_1 state of SM, at the TDDFT//M05-2X/6-31+G(d) level of theory, shows no evidence of this larger geometry change relative to S_0 . Therefore, the calculations provide no reason to suggest a larger change in geometry between S_0 and S_1 in SM than in the SML or SMB analogues.

A final nondynamical contributor to the broadening could be the increasing number of populated conformations in sinapoyl malate. Calculations indeed predict a larger number of low-energy conformers for SM relative to its simpler derivatives but not nearly the number necessary to produce a complete loss of resolved transitions in the spectrum. Furthermore, the composite IR spectra of SM and SDM suggest nearly equal contributions from the same two *syn/anti-cis* conformers found for the rest of the series. The IR spectra were also analyzed at various UV excitation wavelengths in an attempt at shifting the distribution of conformers contributing to the RIDIR spectrum. However, the IR spectrum remained unchanged, consistent with the presence of just two conformers in the jet-cooled spectrum.

4.2.2. Excited State Dynamics. The origin of the spectral broadening in sinapoyl malate, even under jet-cooled conditions, could be the result of facile, intramolecular decay pathways. The introduction of the dicarboxylic acid (or dicarboxylate in SDM), and to some extent the single carboxylate chain in SMB, instigated the dramatic change observed in the UV spectrum. With regard to excited state dynamics, the likely states that would be modulated by this chemical substitution are the $n\pi^*$ states that are conjugated to some degree into the malate side chain, differing from sinapic acid and the simpler derivatives.

In this scenario, SM and SDM could engage in the same decay mechanism as the pCA/MeOpCA molecules, namely, direct internal conversion to an adiabatically lower $^1n\pi^*$ state (n -nonbonding orbital on $C_9=O$).^{20–22} Vertical excitation energy calculations of SM (Table S2, Supporting Information) do not predict a substantial change in the $V(^1\pi\pi^*)$ – $^1n\pi^*$ vertical splitting compared with the other sinapates, with the $^1n\pi^*$ state well above the V' state in vertical excitation. However, the adiabatic energy of the $^1n\pi^*$ state after geometry optimization (e.g., involving elongation of the $C_9=O$ bond and other structural distortions) has been shown to drop the energy of the $n\pi^*$ state dramatically from the vertical/ground state geometry, placing it lower than the bright V' state in pCA and MeOpCA.^{21,22,43} Unfortunately, attempts to optimize the $^1n\pi^*$ state were unsuccessful for SM at the level of theory presented here. Nevertheless, this pathway can be evaluated from an experimental perspective.

If this was a dominant mechanism at play in SM, the adiabatic energy of the $n\pi^*$ state would indeed have to be lower

than S_1 but not well below. The present experiment is sensitive to the $\pi\pi^*/n\pi^*$ energy difference through the ionization step inherent to the R2PI process. According to calculations, the geometry of the ion produced by the R2PI process is not very different than the ground state neutral. If the $^1n\pi^*$ state is populated by fast internal conversion, the excess vibrational energy produced by the process will be carried into the ion. As a result, ionization will require a photon energy from S_1 large enough to reach into this vertical region of the ion. If the energy difference were too large, the R2PI process would be inefficient. However, all indications are that the R2PI process is relatively facile throughout the entire series of sinapate esters, arguing for the state out of which ionization occurs, retaining most of the electronic excitation energy originally placed in it by the first photon. If coupling to the $n\pi^*$ state is a dominant pathway in sinapoyl malate, we estimate that it must occur on a sub-ps time scale to sufficiently lifetime-broaden the vibronic transitions to the extent observed in the spectrum. Calculations of the adiabatic energy of this $^1n\pi^*$ state in SM and adiabatic and vertical ionization energies from that geometry are essential for evaluating this pathway, offering a challenge to theory.

The geometry change associated with the $V(\pi\pi^*)$ state accessed in the sinapates has been proposed in related molecules to lead to efficient *trans*–*cis* isomerization about the C_7 – C_8 double bond.^{23,24,43} This excited state isomerization is a pathway by which the molecule can encounter a conical intersection with the ground state, providing a nonradiative decay pathway to a vibrationally hot ground state species. While this pathway is intriguing to consider in explaining SM excited state dynamics, in the present gas phase experiment, we exclude it as a possibility, as ionization from the ground state surface with vibrational energy equivalent to the UV photon energy is prohibited by Franck–Condon considerations, as just discussed.

Another possible type of state to which the $\pi\pi^*$ state could be coupled is a charge transfer (CT) state. The presence and consequences of coupling of a locally excited state (LE) with a CT state are well-documented in other circumstances.^{40,44} When mixing of a locally excited (LE) state occurs with a CT state, it often leads to complete spectral broadening of the transition to the LE state due to coupling to the dense set of vibronic levels in the adjacent, adiabatically lower CT state that borrows intensity from the bright LE state.⁴⁰ The mixing spreads the $\pi\pi^*$ oscillator strength over a manifold of close-lying CT levels, with a breadth governed by the magnitude of the average coupling matrix elements between the states.

The intriguing possibility offered by SM is that the $^1n\pi^*$ state itself has some charge transfer character to it. On this basis, we postulate that the $n\pi^*$ state and CT state scenarios are not distinct from one another in SM but that the partial CT character of the $n\pi^*$ state contributes to lowering its adiabatic energy relative to the $\pi\pi^*$ state. Thus, the donor–acceptor groups defining the partial charge-transfer character of the $n\pi^*$ state would logically be from the malate side chain to the sinapate aromatic ring, as illustrated by the $n\pi^*$ state electron density difference map shown in Figure 11d. In the figure, blue regions represent gains in electron density while yellow regions indicate depletions. While the two $\pi\pi^*$ transitions involve the loss of electron density from the ring into an antibonding π^* orbital spanning the length of the sinapate, the $n\pi^*$ state clearly shows the transfer of electron density from C_9OO and the first carboxylic acid of the malate group into the antibonding π^* orbital of the sinapate ring.

The UV spectra of SML and SMB provide some confirming evidence for this scenario. First, while the SML UV spectrum still contains a sharp, resolved vibronic structure like that in the alkylated sinapate esters, it also displays some characteristics that hint at the presence of a second state to which the $\pi\pi^*$ state is coupled. First, as Figure 12 demonstrates, the spectrum

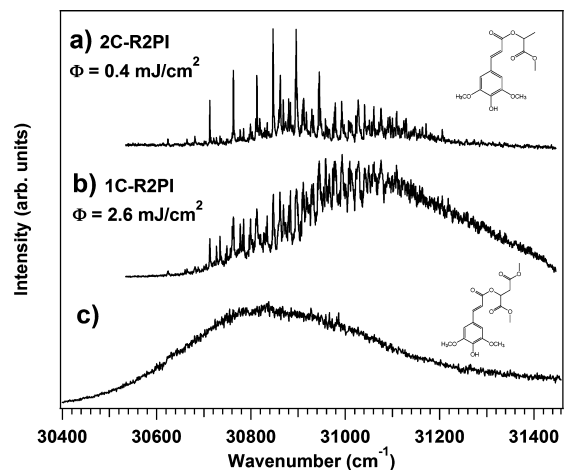


Figure 12. R2PI spectra for SML at (a) low-fluence excitation conditions and (b) intermediate fluence conditions (middle) and (c) R2PI spectrum of SDM at the same intermediate fluence conditions.

of SML showed an unprecedented sensitivity to photon fluence. While the 2C-R2PI spectrum is clearly unsaturated and similar to the simpler derivatives (Figure 12a), an increase in the fluence to that used for acquisition of sharp R2PI spectra of the alkylated esters SA, MS, and IS yields a significant increase in the intensity of an underlying background (Figure 12b). Plotted against the SDM spectrum shown below, the profile of the 1C-R2PI of SML bears a striking resemblance to the sinapoyl malate spectra, perhaps signaling that SML presents an intermediate coupling case in which the mixed LE/CT character of the excited state is apparent by the extreme sensitivity of the spectrum to photon fluence.

A second piece of evidence for the onset of mixing with a CT-like state is in the emission from SML (DFL spectra can be found in the Supporting Information). Sharp transitions back down to Franck–Condon active vibrational levels in the ground state are observed in the DFL spectra of the origin transitions in SML, signaling emission from states of predominantly LE character. However, in comparing the total amount of emission (in photon counts) in this LE Franck–Condon region with the “unperturbed” methyl sinapate DFL spectra (Figure 7), a decrease of at least 2 orders of magnitude in emission is observed despite the expected difference of only 1 order of magnitude based on the total fluorescence signal. One typical feature of CT state mixing/coupling is that loss of emission in the LE Franck–Condon region is accompanied by broadened, red-shifted emission due to the large displacement of the CT geometry from the ground state.^{40,45} In order to search for this component of the emission, the DFL scan was extended out 50 nm to the red of the conformer B origin, yet no discernible emission was found. We surmise that the shifted emission is broadened to the point that the photon counts at the iCCD detector on a per-pixel basis are below the detection limit. It should be noted that, in our DFL detection scheme, a gated intensified CCD with a gate of 10 ns around the laser pulse was

used, thereby precluding the possibility of detecting phosphorescence, and therefore intersystem crossing mechanisms.

Finally, the SMB R2PI spectrum (Figure 8b) shows an absorption profile similar to the intermediate-fluence 1C-R2PI spectrum of SML (Figure 12b), perhaps signaling the initial onset of enhanced LE/CT mixing. We were unable to record DFL spectra for SMB, SM, and SDM due to the lack of laser desorption capabilities in our fluorescence chamber, but direct detection of broad, red-shifted emission in DFL of SM would certainly represent an important future step in confirming a CT-like mechanism. Alternatively, the presence and character of the second excited state responsible for the broadening should be apparent in the time evolution of the photoelectron spectrum.^{46–48} Atomic charges and dipole moments of the three excited states at the ground state geometry were calculated by electrostatic potential (ESP) fitting, also revealing some $n\pi^*$ /CT character, as summarized in the Supporting Information.

Finally, while this discussion has focused attention on the $^1n\pi^*$ excited state, there is also possibly a role for intersystem crossing to the $^3n\pi^*$ state if its energy is also lowered by its partial CT character. The presence of efficient intersystem crossing would be detrimental to SM's role as a UV-B sunscreen, since triplet states could lead to formation of singlet oxygen via triplet–triplet annihilation. However, there is no experimental evidence for formation of a long-lived triplet state either in fluorescence or in two-color R2PI. The presence of a long-lived triplet would be detectable in 2C-R2PI as the delay between the first and second photon was increased. Nevertheless, future investigations that search more carefully for the production of triplet states both in the gas phase and in solution would be worthwhile.

4.2.3. Condensed Phase Spectroscopy. The anomalous broadening observed in the UV spectrum of jet-cooled, gas phase sinapoyl malate provides insight into the decay mechanism intrinsic to the molecule in isolation. While this inherent broadening is unusual under such conditions, the conclusion drawn from this study, namely, that $\pi\pi^*/n\pi^*$ mixing is likely responsible for the observed broadening, is not unique to sinapoyl malate, nor to the gas phase. In fact, in the seminal review by R. M. Hochstrasser more than 40 years ago, the perturbations imposed on $\pi\pi^*$ transitions due to low-lying $n\pi^*$ states in the condensed phase are described in some detail.⁴⁹ Here, several examples are given where $n\pi^*$ states are in close proximity to $\pi\pi^*$ states, such as in nitrogen heterocycles and ketones, and in some cases the ordering of the two states can be modulated by the solvent environment. In cases where an $n\pi^*$ state falls below the bright $\pi\pi^*$ state, spectral broadening of the resolved vibronic bands occurs, at times to the point of complete broadening.⁴⁹ As discussed for sinapoyl malate, this is due to vibronic mixing of the $\pi\pi^*$ levels with background $n\pi^*$ levels. Hochstrasser emphasizes the importance of these interactions, as band broadening in the condensed phase is a good indication of the existence of a lower-energy background state. More specifically, the differences in the orbital character of $\pi\pi^*$ and $n\pi^*$ states (or charge-transfer states) make them primary candidates for mixing, since the Franck–Condon factors that govern vibronic mixing are large when the two states are nearby in energy.⁴⁹ In the case of sinapoyl malate, where the $n\pi^*$ state is itself charge-transfer-like in character, it is possible that such vibronic interactions are enhanced. More recent studies on carbonyl-containing polyenes and carotenoids in the condensed phase, coupled

with *ab initio* calculations, demonstrate the high degree of spectral broadening brought on in $\pi\pi^*$ transitions by a nearby charge-transfer state.⁵⁰

As a first step toward understanding the spectroscopy and photophysics of sinapoyl malate in solution, the isolated, gas phase results presented herein are compared with steady-state absorption (black) and fluorescence (red) spectra of sinapic acid and sinapoyl malate in aqueous solution shown in Figure 13. Spectra were acquired with a Cary 100 UV–vis

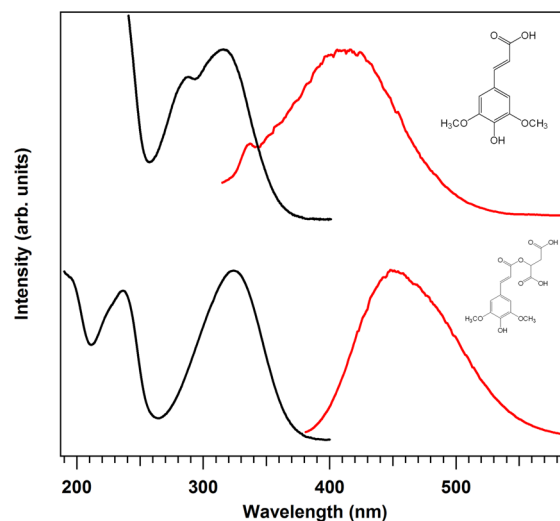


Figure 13. UV absorption spectra (black) and fluorescence spectra (red) taken by excitation at the absorption maximum of sinapic acid (top) and sinapoyl malate (bottom). A solute concentration of $\sim 8 \times 10^{-6}$ M was used to achieve a maximum optical density of ~ 0.1 in a 1 cm path length ($\epsilon_{324 \text{ nm}} \sim 12700 \text{ cm}^{-1} \text{ M}^{-1}$ for sinapoyl malate). The UV-B region spans 280–315 nm.

spectrometer and Fluorolog FL3 fluorescence spectrometer. Methanol and aqueous solution at neutral pH and pH ~ 3 (for increase in $[\text{SM}^-]/[\text{SM}^-]$; vacuolar pH ~ 6.1 ¹²) were used as solvents, with minimal difference between the observed spectra. As anticipated, the well-structured vibronic activity in the gas phase spectrum of sinapic acid is largely lost in solution. The shoulder at 288 nm is some 3200 cm^{-1} above the main $\pi\pi^*$ transition peaked at 318 nm, and could be due to the $n\pi^*$ state. The main band in sinapoyl malate (323 nm) is peaked just slightly red of that in sinapic acid, and is somewhat broader but otherwise similar in appearance. The loss of the shoulder on the short wavelength edge likely signals a red-shift of the $n\pi^*$ transition.

The most striking aspect of the comparison between sinapic acid and sinapoyl malate is in the emission spectra, where a substantial Stokes shift of 127 nm is present in sinapoyl malate (Figure 13, bottom), almost eliminating any spectral overlap between absorption and emission. The fluorescence bands of both sinapates are ~ 100 nm fwhm, and the sinapoyl malate band (450 nm) is red-shifted significantly from sinapic acid (~ 410 nm). When combined, these results point to the active involvement of an intramolecular charge-transfer state in sinapoyl malate in polar solution phase environments, likely the $n\pi^*$ state.

Finally, the fluorescence quantum yields for both sinapic acid and sinapoyl malate in aqueous solution were determined using 9,10-diphenylanthracene as a reference. Both molecules had fluorescence quantum yields of $\Phi \sim 3 \times 10^{-3}$, indicating that

nonradiative processes dominate the excited state decay pathways of both molecules in polar solvents. Future studies that directly detect the intermediate and final states involved in the decay processes, both in the gas phase and in solution, are clearly warranted.^{50,51} Further, while these preliminary condensed phase results suggest the retention of a dominant V–CT interaction even in the presence of hydrogen bonding from polar solvents, jet studies of microsolvated sinapoyl malate:H₂O clusters would be useful in assessing the effects of hydrogen bonding from individual water molecules on the excited states relevant to the nonradiative dynamics. This would present a test case for comparison with the substituted cinnamates, where interactions with only a single water molecule shift the $n\pi^*$ state out of range of the bright V' state, at times dramatically affecting the vibronic features and/or decay pathways.^{20,23}

Taken as a whole, these initial results in aqueous solution provide preliminary support for the notion that the excited state processes ascribed to the isolated sinapoyl malate molecule are also active in solution. At the same time, their preliminary nature motivates further photophysical and photochemical studies that more accurately mimic the *in vivo* environment of the plant itself.

5. CONCLUSIONS

Even under isolated conditions in the gas phase, the sinapate esters, and particularly sinapoyl malate, display properties that justify their role as UV-B screening agents in plants. The electronic transition involved in providing this protection has remarkable absorption efficiency (large oscillator strength) and beautifully matched spectral coverage in the UV-B range. The large absorption coefficient for the transition ensures efficient absorption of photons incident the leaf epidermis (where SM is concentrated). Sufficient wavelength coverage results from a $\pi\pi^*$ transition involving molecular orbitals which extend over the full length of the sinapate group, and produce a geometry change between S₀ and S₁ states that leads to long Franck–Condon progressions involving low-frequency vibrational modes. The result is excitation spectra that are congested and extend over the entire UV-B region. Indeed, the relatively small wavelength range studied here is likely to represent only a fraction of the full absorption profile, with progressions involving C=C and C=O stretch modes, as observed in the DFL spectra of MS (Figure 7).

In increasing the complexity of the ester side chain attached to the sinapate group, increased spectral complexity was observed until complete spectral broadening spanning >1000 cm⁻¹ was reached in SM and SDM. We have argued that the broadening in SM/SDM, and the onset in SML and SMB, can be consistently accounted for by excited state mixing of the V ($\pi\pi^*$) state and a second excited state, most probably the low-energy $n\pi^*$ state, which inherently incorporates significant charge-transfer character. This, coupled with the inherently congested sinapate UV spectrum, yields complete broadening in its UV spectrum even under jet-cooled conditions in the gas phase, a remarkable result. By chemically “deconstructing” sinapoyl malate, and comparing its UV spectral properties with the simpler analogues in this series, a clear progression in behavior is found that illuminates the inherent and unique excited state properties of sinapoyl malate. A cursory analysis of the absorption and fluorescence spectra of sinapoyl malate in aqueous solution demonstrates potential support of this mechanism even in an aqueous environment. These results

taken as a whole suggest a selection of these robust, quantum mechanical features by nature as a means of biologically efficient photoprotection. However, further photochemical studies both in the gas phase and in solution are required to fully investigate the nature of the excited state dynamics and the extent to which the inherent intramolecular processes are modified in their *in vivo* environment in plants.

The presence of an efficient mechanism for intramolecular excited state dynamics leaves open the very important question of the final fate of the energized molecule accessed by absorption of a UV-B photon in sinapoyl malate. If the coupling of the $\pi\pi^*$ state to a second excited state directs the electronic energy back to the ground state via internal conversion, it seems likely that the molecule will collisionally cool on the ground state potential energy surface without undergoing significant photochemistry. This would complete a cycle in which absorption of UV-B radiation leads only to heat dissipated in solution, bringing sinapoyl malate back to its ground state where it can efficiently absorb again. Indeed, this is what one would anticipate of an efficient UV-B sunscreen, in which the plant needn't replenish its supply of the molecule due to photochemical degradation. However, to the best of our knowledge, this has not yet been proven experimentally, nor have the photophysical and photochemical pathways been explored in any detail from a computational viewpoint, calling for future effort along both directions.

■ ASSOCIATED CONTENT

📄 Supporting Information

The experimental procedures for synthesis of MS, IS, SML, SMB, and SDM, experimental details of the laser desorption scheme used in this work, experimental aspects of the double-resonance spectroscopy employed in this work, vibrational frequencies for alkylated sinapates, relaxed potential energy scan about the lowest *syn–anti* interconversion coordinate in SA, structural assignments for SML and SMB, analysis of the small bands to the red of the SML (A) origin, DFL spectra of SML origin transitions, SM/SDM low-energy structures, RIDIR spectra of SM and SDM, Franck–Condon simulations of the V ($\pi\pi^*$) and V' ($\pi\pi^*$) excitations in SA, and TDDFT scaled vertical excitations plotted against experimental R2PI spectra. This material is available free of charge via the Internet at <http://pubs.acs.org>.

■ AUTHOR INFORMATION

Corresponding Author

zwier@purdue.edu

Notes

The authors declare no competing financial interest.

■ ACKNOWLEDGMENTS

The authors gratefully acknowledge Yohei Matsueda for his noteworthy contributions to the synthesis of MS, IS, SML, SMB, and SDM. J.C.D. and T.S.Z. would like to thank Clint Chapple for discussions about sinapoyl malate and its role in UV-B protection in plants. The authors also acknowledge support for this work from the Department of Energy Basic Energy Sciences, Division of Chemical Sciences (DEFG02-96ER14656).

■ REFERENCES

- (1) Bieza, K.; Lois, R. *Plant Physiol.* **2001**, *126*, 1105–1115.

- (2) Booi-James, I. S.; Dube, S. K.; Jansen, M. A. K.; Edelman, M.; Mattoo, A. K. *Plant Physiol.* **2000**, *124*, 1275–1283.
- (3) Landry, L. G.; Chapple, C. C. S.; Last, R. L. *Plant Physiol.* **1995**, *109*, 1159–1166.
- (4) Ren, J.; Dai, W. R.; Xuan, Z. Y.; Yao, Y. N.; Korpelainen, H.; Li, C. Y. *For. Ecol. Manage.* **2007**, *239*, 112–119.
- (5) Demkura, P. V.; Ballare, C. L. *Mol. Plant* **2012**, *5*, 642–652.
- (6) Foyer, C. H.; Lelandais, M.; Kunert, K. J. *Physiol. Plant.* **1994**, *92*, 696–717.
- (7) Jansen, M. A. K.; Gaba, V.; Greenberg, B. M.; Mattoo, A. K.; Edelman, M. *Plant J.* **1996**, *9*, 693–699.
- (8) Jordan, B. R. In *Advances in Botanical Research*; Callow, J. A., Ed.; Academic Press Ltd.: London; San Diego, CA, 1996; Vol. 22, pp 97–162.
- (9) Ruegger, M.; Chapple, C. *Genetics* **2001**, *159*, 1741–1749.
- (10) Chapple, C. C. S.; Vogt, T.; Ellis, B. E.; Somerville, C. R. *Plant Cell* **1992**, *4*, 1413–1424.
- (11) Fraser, C. M.; Chapple, C. *Arabidopsis Book* **2011**, *9*, e0152.
- (12) Sheahan, J. J. *Am. J. Bot.* **1996**, *83*, 679–686.
- (13) Strack, D.; Pieroth, M.; Scharf, H.; Sharma, V. *Planta* **1985**, *164*, 507–511.
- (14) Karpkird, T. M.; Wanichweacharunguang, S.; Albinsson, B. *Photochem. Photobiol. Sci.* **2009**, *8*, 1455–1460.
- (15) Lewis, F. D.; Quillen, S. L.; Elbert, J. E.; Schneider, S.; Geiselhart, P. J. *Photochem. Photobiol.* **1989**, *47*, 173–179.
- (16) Pattanaargson, S.; Limphong, P. *Int. J. Cosmet. Sci.* **2001**, *23*, 153–160.
- (17) Promkatkaew, M.; Suramit, S.; Karpkird, T. M.; Namuangruk, S.; Ehara, M.; Hannongbua, S. *J. Chem. Phys.* **2009**, *131*, 224306.
- (18) Singh, T. S.; Mitra, S.; Chandra, A. K.; Tamai, N.; Kar, S. J. *Photochem. Photobiol.* **2008**, *197*, 295–305.
- (19) Wang, H. B.; Zhai, B. C.; Tang, W. L.; Yu, J. Y.; Song, Q. H. *Chem. Phys.* **2007**, *333*, 229–235.
- (20) Tan, E. M. M.; Hilbers, M.; Buma, W. J. *J. Phys. Chem. Lett.* **2014**, *5*, 2464–2468.
- (21) de Groot, M.; Gromov, E. V.; Koppel, H.; Buma, W. J. *J. Phys. Chem. B* **2008**, *112*, 4427–4434.
- (22) Smolarek, S.; Vdovin, A.; Perrier, D. L.; Smit, J. P.; Drabbels, M.; Buma, W. J. *Am. Chem. Soc.* **2010**, *132*, 6315–6317.
- (23) Tan, E. M. M.; Amirjalayer, S.; Bakker, B. H.; Buma, W. J. *Faraday Discuss.* **2013**, *163*, 321–340.
- (24) Shimada, D.; Kusaka, R.; Inokuchi, Y.; Ehara, M.; Ebata, T. *Phys. Chem. Chem. Phys.* **2012**, *14*, 8999–9005.
- (25) Allais, F.; Martinet, S.; Ducrot, P. H. *Synthesis* **2009**, 3571–3578.
- (26) Quentin, M.; Allasia, V.; Pegard, A.; Allais, F.; Ducrot, P. H.; Favery, B.; Levis, C.; Martinet, S.; Masur, C.; Ponchet, M.; Roby, D.; Schlaich, N. L.; Jouanin, L.; Keller, H. *PLoS Pathog.* **2009**, *5*, 1–9.
- (27) Dean, J. C.; Buchanan, E. G.; Zwier, T. S. *J. Am. Chem. Soc.* **2012**, *134*, 17186–17201.
- (28) Mohamadi, F.; Richards, N. G. J.; Guida, W. C.; Liskamp, R.; Lipton, M.; Cauffield, C.; Chang, G.; Hendrickson, T.; Still, W. C. *J. Comput. Chem.* **1990**, *11*, 440–467.
- (29) Weiner, P. K.; Kollman, P. A. *J. Comput. Chem.* **1981**, *2*, 287–303.
- (30) Zhao, Y.; Truhlar, D. G. *J. Chem. Theory Comput.* **2007**, *3*, 289–300.
- (31) Frisch, M. J.; Trucks, G. W.; Schlegel, H. B.; Scuseria, G. E.; Robb, M. A.; Cheeseman, J. R.; Scalmani, G.; Barone, V.; Mennucci, B.; Petersson, G. A.; Nakatsuji, H.; Caricato, M.; Li, X.; Hratchian, H. P.; Izmaylov, A. F.; Bloino, J.; Zheng, G.; Sonnenberg, J. L.; Hada, M.; Ehara, M.; Toyota, K.; Fukuda, R.; Hasegawa, J.; Ishida, M.; Nakajima, T.; Honda, Y.; Kitao, O.; Nakai, H.; Vreven, T.; Montgomery, J. A., Jr.; Peralta, J. E.; Ogliaro, F.; Bearpark, M.; Heyd, J. J.; Brothers, E.; Kudin, K. N.; Staroverov, V. N.; Kobayashi, R.; Normand, J.; Raghavachari, K.; Rendell, A.; Burant, J. C.; Iyengar, S. S.; Tomasi, J.; Cossi, M.; Rega, N.; Millam, J. M.; Klene, M.; Knox, J. E.; Cross, J. B.; Bakken, V.; Adamo, C.; Jaramillo, J.; Gomperts, R.; Stratmann, R. E.; Yazyev, O.; Austin, A. J.; Cammi, R.; Pomelli, C.; Ochterski, J. W.; Martin, R. L.; Morokuma, K.; Zakrzewski, V. G.; Voth, G. A.; Salvador, P.; Dannenberg, J. J.; Dapprich, S.; Daniels, A. D.; Farkas, O.; Foresman, J. B.; Ortiz, J. V.; Cioslowski, J.; Fox, D. J. *Gaussian 09*; Gaussian, Inc.: Wallingford, CT, 2009.
- (32) Dean, J. C.; Buchanan, E. G.; James, W. H.; Gutberlet, A.; Biswas, B.; Ramachandran, P. V.; Zwier, T. S. *J. Phys. Chem. A* **2011**, *115*, 8464–8478.
- (33) Duschinsky, F. *Acta Physicochim. URSS* **1937**, *7*, 551–566.
- (34) Muller, C. W.; Newby, J. J.; Liu, C. P.; Rodrigo, C. P.; Zwier, T. S. *Phys. Chem. Chem. Phys.* **2010**, *12*, 2331–2343.
- (35) Zilberg, S.; Haas, Y. *J. Chem. Phys.* **1995**, *103*, 20–36.
- (36) Sibert, E. L.; Tabor, D. P.; Dean, J. C.; Kidwell, N. M.; Zwier, T. S. Manuscript in preparation.
- (37) Henderson, J. R.; Muramoto, M.; Willett, R. A. *J. Chem. Phys.* **1964**, *41*, 580.
- (38) Cogan, S.; Zilberg, S.; Haas, Y. *J. Am. Chem. Soc.* **2006**, *128*, 3335–3345.
- (39) Schweke, D.; Baumgarten, H.; Haas, Y.; Rettig, W.; Dick, B. *J. Phys. Chem. A* **2005**, *109*, 576–585.
- (40) Vandantzig, N. A.; Shou, H. S.; Alfano, J. C.; Yang, N. C. C.; Levy, D. H. *J. Chem. Phys.* **1994**, *100*, 7068–7078.
- (41) Dean, J. C.; Navotnaya, P.; Parobek, A. P.; Clayton, R. M.; Zwier, T. S. *J. Chem. Phys.* **2013**, *139*, 144313.
- (42) Rodrigo, C. P.; James, W. H.; Zwier, T. S. *J. Am. Chem. Soc.* **2011**, *133*, 2632–2641.
- (43) Gromov, E. V.; Burghardt, I.; Koppel, H.; Cederbaum, L. S. *J. Phys. Chem. A* **2005**, *109*, 4623–4631.
- (44) Jiang, S.; Levy, D. H. *J. Phys. Chem. A* **2002**, *106*, 8590–8598.
- (45) Fleisher, A. J.; Bird, R. G.; Zaleski, D. P.; Pate, B. H.; Pratt, D. W. *J. Phys. Chem. B* **2013**, *117*, 4231–4240.
- (46) Schalk, O.; Schuurman, M. S.; Wu, G. R.; Lang, P.; Mucke, M.; Feifel, R.; Stolow, A. *J. Phys. Chem. A* **2014**, *118*, 2279–2287.
- (47) Stolow, A. *Int. Rev. Phys. Chem.* **2003**, *22*, 377–405.
- (48) Wolf, T. J. A.; Schalk, O.; Radloff, R.; Wu, G.; Lang, P.; Stolow, A.; Unterreiner, A. N. *Phys. Chem. Chem. Phys.* **2013**, *15*, 6673–6683.
- (49) Hochstrasser, R. M. *Acc. Chem. Res.* **1968**, *1*, 266–274.
- (50) Enriquez, M. M.; Fuciman, M.; LaFountain, A. M.; Wagner, N. L.; Birge, R. R.; Frank, H. A. *J. Phys. Chem. B* **2010**, *114*, 12416–12426.
- (51) Bautista, J. A.; Connors, R. E.; Raju, B. B.; Hiller, R. G.; Sharples, F. P.; Gosztola, D.; Wasielewski, M. R.; Frank, H. A. *J. Phys. Chem. B* **1999**, *103*, 8751–8758.